

VISUALIZATION OF WATER TRANSPORT PATHWAYS IN PLANTS USING DIFFUSION TENSOR IMAGING

Marco L. H. Gruwel^{1, *}, Peter Latta^{2, 3},
Uta Sbotto-Frankenstein², and Patricia Gervai²

¹NRC-CNRC Aquatic and Crop Resource Development, 435 Ellice Avenue, Winnipeg MB R3B 1Y6, Canada

²NRC-CNRC Medical Devices, 435 Ellice Avenue, Winnipeg MB R3B 1Y6, Canada

³Institute for Measurement Science, Slovak Academy of Sciences, Dúbravská Cesta 9, Bratislava SK-84219, Slovakia

Abstract—Magnetic resonance imaging (MRI) is a well established non-invasive technique to retrieve structural information from plants and fruits. Water transport inside these materials has also been studied with MRI, however, the integrate combination of studying both structure and dynamics has hardly been considered. Here it is shown how the anisotropic nature of water diffusion in channels or vessels inside the plant can be used to map these vessels in three dimensions. Diffusion Tensor Imaging (DTI), an MR technique initially introduced to study white matter in mammalian brains, is used to track water transport pathways inside Thompson Seedless grapes and celery as an example.

1. INTRODUCTION

Magnetic resonance (MR) is a well established technique in the field of medical pathology. With mammalian soft tissue consisting for 60–80% of water, MR is an ideal non-invasive technique to acquire anatomical information of tissues and organs. Over the last decade or so MR has been given substantial attention in plant sciences with applications measuring 3D structures [1] and detecting fluid flow [2, 3] in typical vascular structures such as xylem and phloem. A recent overview of high resolution MRI [4] describes the use of

Received 5 November 2012, Accepted 12 December 2012, Scheduled 12 December 2012

* Corresponding author: Marco L. H. Gruwel (marco.gruwel@nrc-cnrc.gc.ca).

MR in plant-environment interactions, gene function, metabolism and plant physiology in general. However, combined MR studies of plant structure and function [5] are far less common than in the biomedical field.

After the introduction of MR Diffusion Tensor Imaging (DTI) [6], it took some time before DTI was implemented as a standard protocol on clinical MR scanners [7, 8]. Since its introduction in the clinic, DTI has gained enormous popularity and has been applied to a large variety of neuroscience studies ranging from traumatic brain injury to multiple sclerosis [9]. DTI measures the anisotropy of water diffusion in 3D, providing anisotropy maps. With the help of tractography algorithms these maps can be used to visualize white matter axons in the brain [10].

Bulk water diffusion is characterized by one constant, the apparent diffusion constant (ADC). When water mobility becomes restricted up to three different constants are needed to describe the path of the diffusion water molecules [11]. Diffusion of water through a cylindrical vessel can be described by two diffusion constants, the larger relating to diffusion parallel to the vessel while the two identical smaller ones relate to diffusion in the radial direction. In general, diffusion can be described by a symmetric 2nd rank tensor (3×3 matrix), meaning that a minimum of 6 diffusion values will completely describe the diffusion of water. The difference in diffusion components is referred to as anisotropy and is characterized by the fractional anisotropy (FA) which basically represents a normalized variance of the diffusion constants [7]. FA maps are the basis for DTI tractography. Asparagus, with a known and well defined fibrous cylindrical morphology, showed the expected water diffusion FA in early diffusion weighted MR experiments [12].

In this paper, we show how water diffusion anisotropy and DTI, in combination with anatomical MR images, can be used to non-invasively visualize the vascular network in fruits and plants. Water diffusion in grape berries and celery will be studied as an example of the potential of DTI in plant science.

2. RESULTS AND DISCUSSION

During its development, flesh of the grape berry obtains water and nutrients through a vascular network. This system consists of a peripheral network in the outer part of the mesocarp, near the exocarp, and a larger axial bundle supplying the seeds.

There is no information available on how the vascular bundles grow in grape berries [13] and how this growth is related to the three stages of berry growth. Some studies have shown a transition in

water flow from primarily xylem to primarily phloem in post-veraison grape berries [14] while other publications do not show any loss of xylem function [15]. However, water is important for the development and composition of fleshy fruit during the growth phases as is an understanding of the underlying vascular network.

Figure 1 shows fractional anisotropy (FA) maps of water movement in a Thompson Seedless grape berry. The images were obtained at 11.7 T using a data matrix of $320 \times 256 \times 38$ and a field of view (FOV) of $40 \text{ mm} \times 26 \text{ mm} \times 21.6 \text{ mm}$, rendering a $125 \mu\text{m} \times 102 \mu\text{m}$ in-plane image resolution in Fig. 1(c). A false colouring scheme is used to obtain a sense of directional preference with respect to the main magnetic field in the MRI system, which is parallel to $A \rightarrow P$,

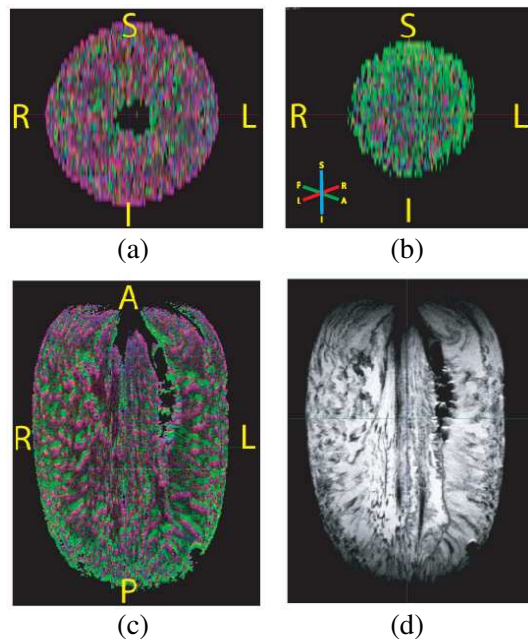


Figure 1. Fractional anisotropy (FA) maps of a Thompson Seedless grape. (a) Axial slice from the top of the grape, the hole from the dried up pedicel is visible. Standard DTI colour coding used in the FA maps is indicated in the left hand bottom corner of (b). The superior-inferior ($S \leftrightarrow I$) direction is coded blue while posterior-anterior ($P \leftrightarrow A$) is coded green and left-right ($L \leftrightarrow R$) is coded red. The orientations are also marked in the images (a)–(c). (b) Axial slice taken at the bottom of the grape. (c) Sagittal slice, showing part of the locule. (d) Shows the same images as (c), but now coded for spin-density using a grey-scale.

coded with blue (see inset Fig. 1(b)). The most striking feature of water mobility in the Thompson Seedless grape is the difference in FA between the top and bottom of the grapes, shown in Figs. 1(a) and (b), respectively. The top of the grape, starting at the berry stem, displays a predominant L \leftrightarrow R (indicated by red) oriented network for water transport while at the bottom this changes to a P \leftrightarrow A direction, coded for by the colour green. The overall FA value calculated for selected regions of interest is not very different, FA = 0.34 ± 0.14 and 0.38 ± 0.15 for top and bottom areas, respectively. Similarly, the mean diffusivity for these regions is $D_m = (1.10 \pm 0.19) \times 10^{-3} \text{ mm}^2 \cdot \text{s}^{-1}$ and $(1.03 \pm 0.23) \times 10^{-3} \text{ mm}^2 \cdot \text{s}^{-1}$ for the top and bottom areas, respectively. For comparison, the diffusion constant for bulk water (at 20°C) is $2.2 \times 10^{-3} \text{ mm}^2 \cdot \text{s}^{-1}$ [11] and for water in tomatoes, depending on the variety and time of year, $1.3\text{--}1.9 \times 10^{-3} \text{ mm}^2 \cdot \text{s}^{-1}$ [16]. Similar values have been reported for studies on fresh cut asparagus [12].

For the anatomical images we selected the echo times such to create contrast that would be helpful to explain observed features in the DTI experiments. Spin-spin (T_2) and spin-lattice (T_1) relaxation times for a variety of grape berries have been reported by Andaur et al. [17]. Their publication focused on the use of MR for volume and °Brix distribution measurements. Pope et al. [18] showed ^1H spin-echo images of grape berries at 300 MHz using echo times of 16 and 54 ms to achieve contrast for their drying studies, the value used here falls in this range.

The origin of the P \leftrightarrow A water transport in the lower hemisphere of the grape can be seen in Figs. 1(c), (d) and Fig. 2. Fig. 1(d) shows the presence of large tissue formations that have a clear axial downward A \rightarrow P direction. The spin-density images in Fig. 2 clearly show a radial tissue structure at the top (Fig. 2(a)), while starting mid-section (Figs. 2(b) and (c)) additional centres, near the visible voids, occur from which tissue grows towards the bottom end of the grape. This tissue formation is responsible for the predominant P \leftrightarrow A water FA, color coded green in Fig. 1. The main reason for the break in the FA symmetry while moving from top to bottom along the long axis of the Thompson Seedless berry is related to the growth pattern of the grape berry. Growth of the berry starts at the stem in a radial fashion, however, once full-grown, the Thompson seedless berry has significantly elongated while the origin of the berry remains near the top, the berry stem. This asymmetric growth is evidenced by the deposition of material in a longitudinal fashion, indicated by the anatomical image in Fig. 1(d). If the berry had grown in a complete radial fashion, the centre of the grape berry would have been located mid-axis.

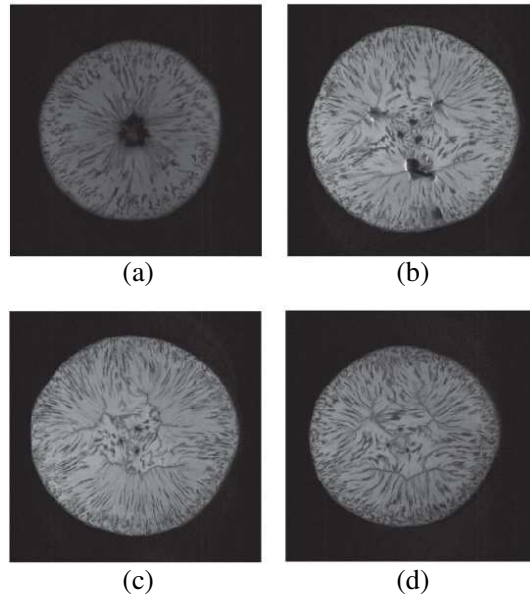


Figure 2. High resolution 2D Spin-Echo anatomical spin-density images of a Thompson Seedless grape obtained at 11.7 T. Imaging parameters: Field of view: $26 \times 26 \text{ mm}^2$, data set of 352×352 pixels, Echo time of 25 ms. Four selected slices are shown, going from top to bottom of the grape from (a) \rightarrow (d).

Figure 3 shows a three dimensional representation of the vascular networks after the application of tractography [19]. For representation purposes the so-called fibres, representing water transport pathways, are represented by tiny cylinders. This figure shows the observations made in Figs. 1 and 2 in a three-dimensional way. Using tractography software, specific regions of interest can be selected for detailed study of the vascular bundles in these areas.

DTI studies are not limited to high magnetic fields and small objects. In Figs. 4(a), (b) a low resolution DTI experiment on a celery plant is shown. The celery plant, with roots removed, was obtained from a local grocery store and imaged in a 3 T clinical scanner using a human RF head coil. The data matrix was $128 \times 128 \times 74$ with a field of view (FOV) of $240 \text{ mm} \times 240 \text{ mm} \times 141 \text{ mm}$, rendering a $1.88 \text{ mm} \times 1.88 \text{ mm}$ in-plane image resolution and 1.9 mm thick slices in the I \leftrightarrow S direction. In Fig. 4(a), the results of tractography are superimposed on the 3D spin-density image of the celery plant, using a cut-out. The FA of the major water transport vessels in celery, shown



Figure 3. Three dimensional representation of the grape berry vasculature obtained from tractography of data from Fig. 1. The orientation of the grape is indicated in the left bottom corner. Colour coding used in tractography is the same as in for the FA maps.

in Fig. 4(b), is coded blue, indicating the I \leftrightarrow S direction for water transport, as expected. Fig. 4(c) shows axial images of a bundle of smaller stalks, obtained with micro imaging at 11.7 T. The arrows in the figure indicate the position of some of the big xylem vessels which are used for water transport. These are the bundles shown in Fig. 4(a) of the celery plant.

The b-value used in DTI experiments is determined by the square of the diffusion gradient strength and the diffusion time. With the increase in diffusion time, signal intensity is being reduced due to diffusion, as a consequence the signal to noise ratio of the image will reduce. Increased gradient strength on the other hand might cause unwanted artifacts, e.g., eddy currents. Our experience with DTI on humans, animals and plants indicate that b-values in the range of 500–1000 s \cdot mm⁻² provide good quality images and reliable DTI parameters, e.g., FA-values and diffusion constants. In the case of high b-values (> 1000 s \cdot mm⁻²) water compartmentation, or restricted diffusion, or a combination of these, might affect the data processing, resulting in changing FA values with changing b-value. However, Hui et al. [20] reported that FA values were less susceptible to changes in b-value than other parameters.

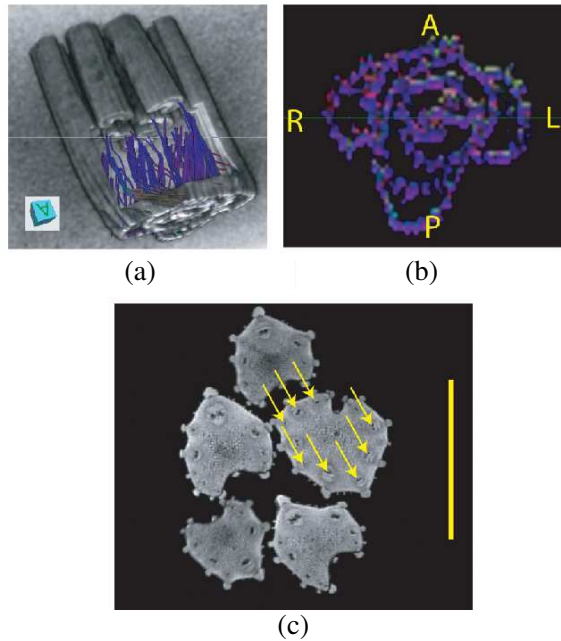


Figure 4. (a) low resolution celery image, obtained at 3 T, with reconstructed fibres for the bottom part of the plant embedded in the cut-out. (b) Axial FA map of the bottom part of a celery plant, using the same notation as in Fig. 1, indicating water transport in the $S \leftrightarrow I$ direction. (c) High resolution spin echo micro images obtained at 11.7 T on small stalks. Some of the main transport vessels are indicated by arrows. The yellow bar on the right hand side of the image indicates 1 cm.

Using Thompson Seedless grapes and celery we have shown DTI and tractography can be used to obtain structural information on water transport in plants and fruit. Simple FA maps obtained from DTI data already display the main transport characteristics while tractography details connectivity in 3D.

3. EXPERIMENTAL PROCEDURES

All micro-imaging MR experiments were performed on an Avance DRX Bruker console (Bruker, Karlsruhe, Germany) using a 72-mm self-shielded gradient system SGRAD 123/72/S (o.d./i.d.) (Magnex, UK) installed in a vertical bore, 11.7 T magnet (Magnex, UK). Experiments

were performed using a Doty (Columbia, SC) 34 mm (i.d.) DSI-863, linear, Litz RF-coil. Gradient echo and Spin-echo experiments were performed to acquire scout and anatomical images. Spin-echo images of grape berries were acquired with $TR = 2$ s, $TE = 25$ ms, $NA = 2$, $FOV = 26 \times 26$ mm² using a data matrix of 325×352 data points, a 1 mm slice thickness and totalling 19 min of acquisition time. For the Spin-echo images of small celery stalks in Fig. 4(c) we used the same imaging parameters, with the exception of $FOV = 28 \times 28$ mm². A modified diffusion weighted spin-echo sequence, using a b -value of $800 \text{ s} \cdot \text{mm}^{-2}$ with 6 orthogonal gradient directions, was used for the acquisition of the DTI data. DTI parameters used were $TR = 20$ s, $TE = 26$ ms, $NA = 2$, $FOV = 40 \times 26 \times 21.6$ mm³ (38 slices of 0.6 mm thickness) using an in-plane data matrix of 320×286 points, totalling 20 hours of acquisition time. Experiments on a whole celery plant were performed on a 3T clinical scanner (Tim Trio; Siemens Medical Solutions, Erlangen, Germany) using a standard head RF-coil. DTI data was acquired using a single-shot Spin Echo EPI (MDDW) sequence for 20 gradient directions following an icosahedral scheme and a b -value of $600 \text{ s} \cdot \text{mm}^{-2}$. Sequence parameters for the 3T DTI measurements were $TR = 9100$ ms, $TE = 93$ ms, $NA = 4$, $FOV = 24 \times 24 \times 14$ cm³ (74 slices of 1.89 mm thickness) using an in-plane data matrix of 128×128 points, parallel imaging using GRAPPA with an effective acceleration factor 2 and a total acquisition time of 20 min.

Both the Thompson Seedless grapes and the celery were obtained from a local grocery just prior to the experiment.

DTI and fibre tract data processing was performed with MedINRIA software [21] from INRIA, Asclepios Research project, 06902 Sophia Antipolis CEDEX, France.

REFERENCES

1. Koeckenberger, W., C. De Panfilis, D. Santoro, P. Dahiya, and S. Rawsthorne, "High resolution NMR microscopy of plants and fungi," *J. Microsc.*, Vol. 214, No. 2, 182–189, 2004.
2. Scheenen, T., A. Heemskerk, A. De Jager, F. Vergeldt, and H. Van As, "Functional imaging of plants: A nuclear magnetic resonance study of a cucumber plant," *Biophys. J.*, Vol. 82, No. 1, Pt. 1, 481–492, 2002.
3. Scheenen, T. W. J., F. J. Vergeldt, A. M. Heemskerk, and H. Van As, "Intact plant magnetic resonance imaging to study dynamics in long-distance sap flow and flow-conducting surface area," *Plant Physiol.*, Vol. 144, No. 2, 1157–1165, 2007.

4. Borisjuk, L., H. Rolletschek, and T. Neuberger, "Surveying the plant's world by magnetic resonance imaging," *Plant J.*, Vol. 70, No. 1, 129–146, 2012.
5. Jahnke, S., M. I. Menzel, D. Van Dusschoten, G. W. Roeb, J. Buehler, S. Minwuyelet, P. Bluemler, V. M. Temperton, T. Hombach, M. Streun, S. Beer, M. Khodaverdi, K. Ziemons, H. H. Coenen, and U. Schurr, "Combined MRI-PET dissects dynamic changes in plant structures and functions," *Plant J.*, Vol. 59, No. 4, 634–644, 2009.
6. Basser, P. J., J. Mattiello, and D. Le Bihan, "MR diffusion tensor spectroscopy and imaging," *Biophys J.*, Vol. 66, No. 1, 259–267, 1994.
7. Le Bihan, D., J. F. Mangin, C. Poupon, C. A. Clark, S. Pappata, N. Molko, and H. Chabriet, "Diffusion tensor imaging: Concepts and applications," *J. Magn. Reson. Imaging*, Vol. 13, No. 4, 534–546, 2001.
8. Tournier, J.-D., S. Mori, and A. Leemans, "Diffusion tensor imaging and beyond," *Magn. Reson. Med.*, Vol. 65, No. 6, 1532–1556, 2011.
9. Ciccarelli, O., M. Catani, H. Johansen-Berg, C. Clark, and A. Thompson, "Diffusion-based tractography in neurological disorders: Concepts, applications, and future developments," *Lancet Neurol.*, Vol. 7, No. 8, 715–727, 2008.
10. Lazar, M., "Mapping brain anatomical connectivity using white matter tractography," *NMR Biomed.*, Vol. 23, No. 7, 821–835, 2010.
11. Gruwel, M. L. H., P. K. Ghosh, P. Latta, and D. S. Jayas, "On the diffusion constant of water in wheat," *J. Agric. Food Chem.*, Vol. 56, No. 1, 59–62, 2008.
12. Boujraf, S., R. Luybaert, H. Eisendrath, and M. Osteaux, "Echo planar magnetic resonance imaging of anisotropic diffusion in asparagus stems," *MAGMA*, Vol. 13, No. 2, 82–90, 2001.
13. Chatelet, D. S., T. L. Rost, M. A. Matthews, and K. A. Shackel, "The peripheral xylem of grapevine (*Vitis vinifera*) berries. 2. Anatomy and development," *J. Exp. Bot.*, Vol. 59, No. 8, 1997–2007, 2008.
14. Greenspan, M., K. Shackel, and M. A. Matthews, "Developmental changes in the diurnal water budget of the grape berry exposed to water deficits," *Plant, Cell Environ.*, Vol. 17, 811–820, 1994.
15. Bondada, B. R., M. A. Matthews, and K. A. Shackel, "Functional xylem in the post-veraison grape berry," *J. Exp. Bot.*, Vol. 56,

- No. 421, 2949–2957, 2005.
16. Duva, F. P., M. Cambert, and F. Mariette, “NMR study of tomato pericarp tissue by spin-spin relaxation and water self-diffusion,” *Appl. Magn. Reson.*, Vol. 28, 29–40, 2005.
 17. Andaur, J. E., A. R. Guesalaga, E. E. Agosin, M. W. Guarini, and P. Irarrázaval, “Magnetic resonance imaging for nondestructive analysis of wine grapes,” *J. Agric. Food Chem.*, Vol. 52, 165–170, 2004.
 18. Pope, J. M., D. Jonas, and R. R. Walker, “Applications of NMR micro-imaging to the study of water, lipid, and carbohydrate distribution in grape berries,” *Protoplasma*, Vol. 173, 177–186, 1993.
 19. Fillard, P., X. Pennec, V. Arsigny, and N. Ayache, “Clinical DT-MRI estimation, smoothing, and fiber tracking with log-Euclidean metrics,” *IEEE Trans. Med. Imaging*, Vol. 26, No. 11, 1472–1482, 2007.
 20. Hui, E. S., M. M. Cheung, K. C. Chan, and E. X. Wu, “B-value dependence of DTI quantitation and sensitivity in detecting neural tissue changes,” *Neuroimage*, Vol. 49, 2366–2374, 2010.
 21. Fillard, P. and N. Toussaint, “DTI processing and analysis with MedINRIA,” *Proc. Intl. Soc. Mag. Reson. Med.*, Vol. 19, 4030, 2011.